

# *Ab Initio* Linear Response Study of SrTiO<sub>3</sub>

Chris LaSota, Cheng-Zhang Wang, Rici Yu, and Henry Krakauer

*Department of Physics, College of William and Mary, Williamsburg, Virginia 23187-8795*

(March 5, 1996)

## Abstract

The lattice instabilities of perovskite structure oxides are responsible for many of their interesting properties, such as temperature-dependent ferroelectric phase transitions. First-principles calculations using linear response theory provide an accurate means to determine the lattice dynamics throughout the entire Brillouin zone (BZ). Using the LAPW linear response method [1], we have previously carried out such a study on ferroelectric KNbO<sub>3</sub> [2]. We present here the results of a similar investigation for cubic SrTiO<sub>3</sub>. While KNbO<sub>3</sub> has only ferroelectric-type instabilities, SrTiO<sub>3</sub> exhibits both ferroelectric (FE) and antiferrodistortive (AFD) instabilities. We correctly predict the known instability at the R-point in the Brillouin zone, which is responsible for the AFD phase transition to the tetragonal structure at about 105 K. Furthermore, the phase space of the ferroelectric instability is greatly reduced compared to KNbO<sub>3</sub>. Antiferrodistortive instabilities exist in one-dimensional cylindrical tubes extending along the entire R-M-R line in the Brillouin zone. The essentially 1-D character of these tubes corresponds to real-space planar instabilities characterized by rotations of oxygen octahedra.

PACS numbers: 63.10.+a, 77.80.-e, 77.84.Dy

Typeset using REVTeX

## I. INTRODUCTION

Strontium titanate has been the subject of ongoing theoretical and experimental investigation for over 30 years, due to its unusual properties. In cubic perovskite structure  $\text{KNbO}_3$  and  $\text{BaTiO}_3$ , transitions to ferroelectric phases occur as the temperature is lowered.  $\text{SrTiO}_3$ , which has the same high-temperature structure, behaves somewhat differently in that it undergoes an antiferrodistortive (AFD) transition as the temperature drops below about 105 K [3]. This is due to a softening of the lowest frequency triply degenerate zone-corner R-point vibrational mode of lowest energy [4,5]. In this mode, the Sr and Ti atoms remain fixed, while the oxygen octahedra rotate about one of the cubic axes passing through the Ti atom. The sense of the rotation is opposite in adjacent cells in all directions as shown in Fig. 1. As the temperature continues to drop below the AFD transition, there is a sharp rise in the value of the static dielectric constant. This increase appears to follow a Curie-Weiss law consistent with an impending ferroelectric (FE) transition at about 20 K. With decreasing temperature, however, the static dielectric constant saturates at a high value, and the material does not become ferroelectric even at the lowest temperatures [6,7]. It has been suggested that the FE transition is inhibited due to quantum paraelectric behavior, in which the zero-point motion of the atoms suppresses the long-range FE order [8,9]. It is thus of great interest to characterize the structural instabilities of  $\text{SrTiO}_3$ . The present work is concerned with the wavevector dependence of structural instabilities in  $\text{SrTiO}_3$ , obtained from first-principles calculations, and their interpretation in light of previous similar calculations on  $\text{KNbO}_3$ .

## II. METHODS

Our calculations are carried out utilizing the LAPW formalism [10], wherein the wave functions, charge density, and potential all have dual representations. Within non-overlapping muffin-tin spheres, these quantities are expanded as numerical radial functions

times spherical harmonics, while in the interstitial region, a plane wave representation is used. This method has several attractive features, such as employing an unbiased representation in the interstitial region and the ability to easily treat first-row and d-band atoms. The major drawback presented by this method is the use of position-dependent basis functions. This introduces correction terms when computing such quantities as the forces on the atoms [11], and thus complicates the computer programs. In order to investigate all possible soft phonon modes in a particular substance, we must map out the dispersion curves throughout the Brillouin zone. This is accomplished quite easily using linear response theory [1,12]. In linear response theory, the total variational energy is expanded to second order as a function of the equilibrium charge density and the first-order change in the charge density:

$$E_T = E^{(0)}[\rho^{(0)}] + \lambda E^{(1)}[\rho^{(0)}] + \lambda^2 E^{(2)}[\rho^{(1)}] + \dots \quad (1)$$

Minimizing this energy with respect to the first-order change in the charge density yields a pair of equations which must be solved self-consistently:

$$\rho^{(1)} = \sum_{i=1}^N \psi_i^* \psi_i^{(1)}, \quad (2)$$

$$\left( H^{(0)} - \varepsilon_i^{(0)} \right) \psi_i^{(1)} = - \left( V_{eff}^{(1)}[\rho^{(1)}] \right) \psi_i^{(0)}. \quad (3)$$

The equations are the first-order analogs of the usual local density approximation (LDA) equations, i.e. this is an exact theory; there are no approximations beyond LDA.

The dynamical matrix elements for a given wavevector  $\vec{\mathbf{q}}$  are found via the first-order forces. The forces on all the atoms are calculated for at most  $3N$  selected atomic displacements at each wavevector, where  $N$  is the number of atoms in the primitive cell. To map the phonon dispersion curves throughout the Brillouin zone, we compute the dynamical matrix on a uniform grid of  $q$ -points. The short-range real-space force constants are then obtained by Fourier transform, after subtracting out the analytic long-range dipolar contribution. By inverse Fourier transform, adding in the long-range part, we may compute the dynamical matrix at an arbitrary  $q$ -point. For the  $\text{SrTiO}_3$  calculations, we have used a  $6 \times 6 \times 6$  mesh of

q-points. Exploiting symmetry, we had to compute the dynamical matrix at only 20 q-points in the irreducible BZ wedge. Typically, at each q-point, 3N=15 self-consistent calculations were performed.

The electronic contribution to the static dielectric constant,  $\epsilon_\infty$ , is determined from the induced potential:

$$\hat{\mathbf{q}} \cdot \epsilon_\infty \cdot \hat{\mathbf{q}} = \lim_{\mathbf{q} \rightarrow \mathbf{0}} \left[ 1 - \frac{V_{ind}(\vec{\mathbf{q}})}{V_{total}(\vec{\mathbf{q}})} \right]. \quad (4)$$

The macroscopic polarization at long wavelength is given by the first order change in the charge density

$$P = \lim_{\vec{\mathbf{q}} \rightarrow 0} \frac{i}{q} \rho^{(1)}(\vec{\mathbf{q}}), \quad (5)$$

and from this we can compute the Born effective charges

$$Z_{\alpha,\beta}^*(j) = Z_j + \Omega \left. \frac{\partial P_\alpha}{\partial \tau_\beta(j)} \right|_{\vec{\mathbf{E}}=0}. \quad (6)$$

Here,  $Z_j$  is the ionic contribution, and the second term is the unit cell volume times the derivative of the polarization with respect to displacements of the atoms at zero electric field.

### III. RESULTS

We first performed self-consistent total-energy calculations in the cubic phase to determine the equilibrium properties. Table I lists the theoretical lattice parameters and bulk moduli for the present work, along with those of King-Smith and Vanderbilt [13], as well as some experimental values. Our calculated lattice parameter is only 0.4% larger than the experimental value, so we have used the theoretical value in the following calculations. The electronic component of the static dielectric constant,  $\epsilon_\infty$ , was found to be 6.63, which is about 28% larger than an experimental value of 5.18. This kind of overestimation of  $\epsilon_\infty$  is typical of LDA calculations [14,15].

Table II lists the Born effective charges ( $Z^*$ ) for each type of atom. For Sr and Ti, the values are isotropic, while for the O atoms, there are two distinctive values—for displacements along and perpendicular to the Ti-O bonds, labeled  $\parallel$  and  $\perp$ , respectively. Also listed are the results of calculations by Zhong, King-Smith, and Vanderbilt [16]. Respective theoretical lattice parameters were used for the calculations. Note the anomalously large values for  $Z^*(\text{Ti})$  and  $Z^*(\text{O})_{\parallel}$  due to strong covalent interactions between these atoms [17,18]. We find that our results are generally in good agreement with those of Zhong *et al.* [16].

Table III compares our zone-center optic phonon frequencies with planewave pseudopotential frozen phonon calculations and experimental data. Both calculations find unstable transverse optic (TO) modes at the  $\Gamma$ -point with imaginary frequencies. The longitudinal optic (LO) mode frequencies were obtained using

$$D_{i\alpha,j\beta}^{LO} = D_{i\alpha,j\beta}^{TO} + \frac{4\pi e^2}{\Omega\sqrt{M_i M_j}} \frac{(\mathbf{Z}_i^* \cdot \hat{\mathbf{q}})_{\alpha} (\mathbf{Z}_j^* \cdot \hat{\mathbf{q}})_{\beta}}{\varepsilon_{\infty}}, \quad (7)$$

where  $D^{TO}$  is the zone-center dynamical matrix without macroscopic field,  $\mathbf{Z}_i^*$  and  $M_i$  are the Born effective charge tensor and mass for atom  $i$ ,  $\Omega$  is the volume of the unit cell,  $\alpha, \beta$  are Cartesian indices, and  $\hat{\mathbf{q}}$  is a unit wavevector. The results of Zhong, King-Smith, and Vanderbilt were determined using  $\varepsilon_{\infty}=5.18$  from experiment, whereas we used our larger calculated value of 6.63. To determine what effect  $\varepsilon_{\infty}$  has on the LO mode eigenvalues, a second calculation was performed using  $\varepsilon_{\infty}=5.18$ . The highest LO mode is most sensitive, changing from 751 to 832  $\text{cm}^{-1}$ , while the other two are fairly insensitive.

We present the calculated phonon dispersion curves for cubic  $\text{SrTiO}_3$  plotted along high-symmetry directions in Fig. 2. The  $\Gamma\text{X}$ ,  $\Gamma\text{M}$ , and  $\Gamma\text{R}$  lines correspond to the  $\langle 100 \rangle$ ,  $\langle 110 \rangle$ , and  $\langle 111 \rangle$  directions, respectively. Imaginary frequencies are represented by negative values. The character of the modes at the zone-center and zone-boundaries has been labeled according to the notation by Cowley [19]. The form of some of our lower dispersion curves for the  $\Gamma\text{M}$  and  $\Gamma\text{R}$  directions is roughly in accordance with data reported by Shirane and Yamada at 120 K [5], including an apparent softening of a mode at the R-point. Similar behavior is seen at the M-point, but the lowest zone-boundary phonon mode  $\text{M}_3$  was reported as being

temperature-independent through the AFD transition.

Since we are mainly concerned with structural instabilities and how they relate to the observed phase transitions, we will focus on the portions of the dispersion curves which lie below the  $\omega=0$  dashed line in Fig. 2. Note the large phase space for unstable modes. Our calculations indicate unstable modes at the R-point ( $R_{25}$ ), zone-center ( $\Gamma_{15}$ ), and M-point ( $M_3$ ). These instabilities are of two types: FE ( $\Gamma_{15}$ ), and AFD ( $R_{25}$  and  $M_3$ ). In the  $\Gamma_{15}$  TO mode, Ti atoms move parallel to one of the Ti-O bonds, and the oxygen octahedra move in the opposite direction. This mode is responsible for the FE transitions in materials like BaTiO<sub>3</sub> and KNbO<sub>3</sub> [20,21]. The  $M_3$  mode is nearly identical to the  $R_{25}$  mode in Fig. 1 with one exception. The rotation of the octahedra is in the *same* sense in neighboring cells along the vertical c-axis, but remains opposite in the horizontally adjacent cells. The dispersion curves of Fig. 2 show  $|\omega(\Gamma_{15})| < |\omega(R_{25})|$ , suggesting that LDA may find a FE structure (rhombohedral?) to be lower in energy than the AFD tetragonal structure. Of course experimentally there is no observed transition from AFD to FE phase, although it is seen in the Monte Carlo simulations of Zhong and Vanderbilt [22]. Recently, they have included quantum fluctuation effects into these simulations, and find the FE transition completely suppressed [23,24].

The regions of instability in the BZ are better visualized in Fig. 3, in which isosurfaces, corresponding to  $\omega=0$ , are shown for the lowest unstable phonon modes. The cubic BZ, with  $\Gamma$  at the center, is also shown. The inner isosurface is centered at the  $\Gamma$ -point, and can be visualized as three interpenetrating “cookies”, one perpendicular to each Cartesian direction. The region of FE-type instability is interior to this first isosurface. Between the first and the second isosurface, which lies near the zone edges, all modes are stable. Thus unstable modes are present along the entire R-M-R edge of the BZ. In a repeated-zone scheme, this isosurface would appear as narrow cylindrical tubes extending from R-M-R.

We now discuss the current work in light of results for similar calculations on cubic KNbO<sub>3</sub> by Yu and Krakauer [2]. The dispersion curves of KNbO<sub>3</sub> also reveal a large region of instability for the lowest modes. In contrast to SrTiO<sub>3</sub>, a soft mode is present at the

X-point, and the lowest R-point mode is stable. Although M-point instabilities exist for both materials, the character of these modes is quite different. In  $\text{KNbO}_3$  the motion of the atoms is the same as for the zone-center  $\Gamma_{15}$  mode with the exception that two O atoms perpendicular to the motion remain fixed, i.e. it is essentially the “ferroelectric” soft mode. In  $\text{SrTiO}_3$ , the motion is a rotation of the octahedra as described above. A similar  $\omega=0$  isosurface plot for  $\text{KNbO}_3$  shows that the FE instability extends from the zone-center all the way to the zone-boundary within planar slab-like regions. An AFD instability was not present in the  $\text{KNbO}_3$  calculations. Notice that in  $\text{SrTiO}_3$ , the large planar regions of FE instability have shrunk down to three interpenetrating “cookies”, and the phase space corresponding to the FE character is greatly reduced.

Because the regions of instability in  $\text{KNbO}_3$  reside in slabs which extend across the entire BZ, any linear combination of phonon modes within one of these regions will also be unstable. In a real-space picture, unstable atomic chain-like structures can develop, where the Nb atoms are all displaced in the same direction [2,20]. The width of the slab-like regions in  $\text{KNbO}_3$  indicates the length of the shortest such chains to be about 5 lattice parameters [2]. We can perform a similar qualitative analysis of the real-space motion of the atoms in  $\text{SrTiO}_3$  from its isosurface plot. Since there exists a continuous instability extending from R-M-R, linear combinations of phonon modes along this cylindrical tube-like region will also be unstable. The character of modes along the zone edges is one of rotating oxygen octahedra; thus, an unstable thin disk or planar region could form in real space wherein the octahedra are rotated in opposite senses in neighboring cells, with the surrounding regions remaining undisplaced. From the width of the cylinders containing the instability, we estimate the smallest radius of the real-space disks to be approximately 3–5 lattice parameters. Because of the sensitive dependence of the soft modes on volume, it is possible that these cylinders may pinch off at the M-point at slightly reduced volumes. We have not investigated this yet.

## IV. SUMMARY

In summary, we performed first-principles linear response calculations of the wavevector dependence of structural instabilities for cubic SrTiO<sub>3</sub>. In comparison with previous work on KNbO<sub>3</sub>, we notice three differences. First, calculations on KNbO<sub>3</sub> show a ferroelectric-type instability only, while SrTiO<sub>3</sub> calculations exhibit both FE and AFD instabilities. Second, the phase space of the two-dimensional FE instability (corresponding to chains in real space) is greatly reduced and no longer extends to the zone-edges as in KNbO<sub>3</sub>, but is restricted to the interior of a region likened to three inter-penetrating “cookies”. Third, the AFD instability occupies a rather large region of phase space extending along the entire BZ edges in cylindrical tubes. The essentially 1-D character of these tubes corresponds to real-space planar instabilities characterized by rotations of the oxygen octahedra. Future calculations for SrTiO<sub>3</sub> in the tetragonal phase (below the AFD transition) will be required in order to investigate any instabilities—especially ferroelectric instabilities—that persist.

## ACKNOWLEDGMENTS

This research was supported by Office of Naval Research grant N00014-94-1-1044. C.-Z. Wang was supported by National Science Foundation Grant DMR-9404954. Computations were carried out at the Cornell Theory Center.



## REFERENCES

- [1] R. Yu and H. Krakauer, Phys. Rev. B **49**, 4467 (1994).
- [2] R. Yu and H. Krakauer, Phys. Rev. Lett. **74**, 4067 (1995).
- [3] H. Unoki and T. Sakudo, J. Phys. Soc. Japan **23**, 546 (1967).
- [4] P. A. Fleury, J. F. Scott, and J. M. Worlock, Phys. Rev. Lett. **21**, 16 (1968).
- [5] G. Shirane and Y. Yamada, Phys. Rev. **177**, 858 (1969).
- [6] T. Sakudo and H. Unoki, Phys. Rev. Lett. **26**, 851 (1971).
- [7] R. Viana, P. Lunkenheimer, J. Hemberger, R. Böhmer, and A. Loidl, Phys. Rev. B **50**, 601 (1994).
- [8] K. A. Müller and H. Burkard, Phys. Rev. B **19**, 3593 (1979).
- [9] K. A. Müller, W. Berlinger, and E. Tosatti, Z. Phys. B **84**, 277 (1991).
- [10] O. K. Andersen, Phys. Rev. B **12**, 3060 (1975); E. Wimmer, H. Krakauer, M. Weinert, and A. J. Freeman, Phys. Rev. B **24**, 864 (1981); S.-H. Wei and H. Krakauer, Phys. Rev. Lett. **55**, 1200 (1985); D. J. Singh, *Planewaves, Pseudopotentials and the LAPW Method* (Kluwer Academic Publishers, Massachusetts, 1994).
- [11] R. Yu, D. Singh, and H. Krakauer, Phys. Rev. B **43**, 6411 (1991).
- [12] S. Baroni, P. Giannozzi, and A. Testa, Phys. Rev. Lett. **59**, 2662 (1987).
- [13] R. D. King-Smith and D. Vanderbilt, Phys. Rev. B **49**, 5828 (1994).
- [14] S. de Gironcoli, S. Baroni, and R. Resta, Phys. Rev. Lett. **62**, 2853 (1989).
- [15] C. Z. Wang, R. Yu, and H. Krakauer, Phys. Rev. B **53**, 5430 (1996).
- [16] W. Zhong, R. D. King-Smith, and D. Vanderbilt, Phys. Rev. Lett. **72**, 3618 (1994).
- [17] R. E. Cohen and H. Krakauer, Phys. Rev. B **42**, 6416 (1990).

- [18] R. E. Cohen, Nature (London) **358**, 136 (1992).
- [19] R. A. Cowley, Phys. Rev. **134**, A981 (1964).
- [20] R. Comes, M. Lambert and A. Guiner, Solid State Commun. **6**, 715 (1968).
- [21] T. P. Dougherty *et al.*, Science **258**, 770 (1992).
- [22] W. Zhong and D. Vanderbilt, Phys. Rev. Lett. **74**, 2587 (1995).
- [23] W. Zhong and D. Vanderbilt, Phys. Rev. B (in press).
- [24] D. Vanderbilt, W. Zhong, J. Padilla, and A. Garcia (this volume).
- [25] J. L. Servoin, Y. Luspain, and F. Gervais, Phys. Rev. B **22**, 5501 (1980).

## FIGURES

FIG. 1. Motion of the oxygen atoms in the zone-corner  $R_{25}$  phonon mode. The Ti atoms lie inside the octahedra and do not move. The Sr atoms are also fixed but are not shown. The octahedra rotate about the c-axis in opposite senses in all adjacent cells.

FIG. 2. Calculated phonon dispersion curves for cubic  $\text{SrTiO}_3$  at the theoretical lattice constant.

FIG. 3. Zero-frequency isosurfaces of the lowest unstable phonon modes over the entire BZ. The  $\Gamma$ -point is located at the center of the cube. Unstable modes exist inside the central surface and along the full length of the zone-edges.

## TABLES

TABLE I. Equilibrium properties determined by calculations and experiment for SrTiO<sub>3</sub>.

	Lattice parameter $a$ (a.u.)	Bulk modulus (GPa)
Present	7.412	190
PW <sup>a</sup>	7.303	200
Exp. <sup>b</sup>	7.380	
Exp. <sup>c</sup>		179±6

<sup>a</sup>Planewave ultrasoft-pseudopotential calculation by King-Smith and Vanderbilt [13].

<sup>b</sup>Wyckoff, *Crystal Structures*, vol. 2, 2nd ed. (1964).

<sup>c</sup>T. Mitsui *et al.*, Landolt-Bornstein Series, Group III, vol. 3 (1969).

TABLE II. Born effective charges for cubic SrTiO<sub>3</sub>.

	Present	PW-BP <sup>a</sup>
Lattice parameter (a.u.)	7.412	7.303
Z*(Sr)	2.55	2.54
Z*(Ti)	7.56	7.12
Z*(O) <sub>  </sub>	-5.92	-5.66
Z*(O) <sub>⊥</sub>	-2.12	-2.00

<sup>a</sup>Planewave Berry phase calculation by Zhong *et al.* [16].

TABLE III. Calculated zone-center optic phonon frequencies (in  $\text{cm}^{-1}$ ) in cubic  $\text{SrTiO}_3$ .

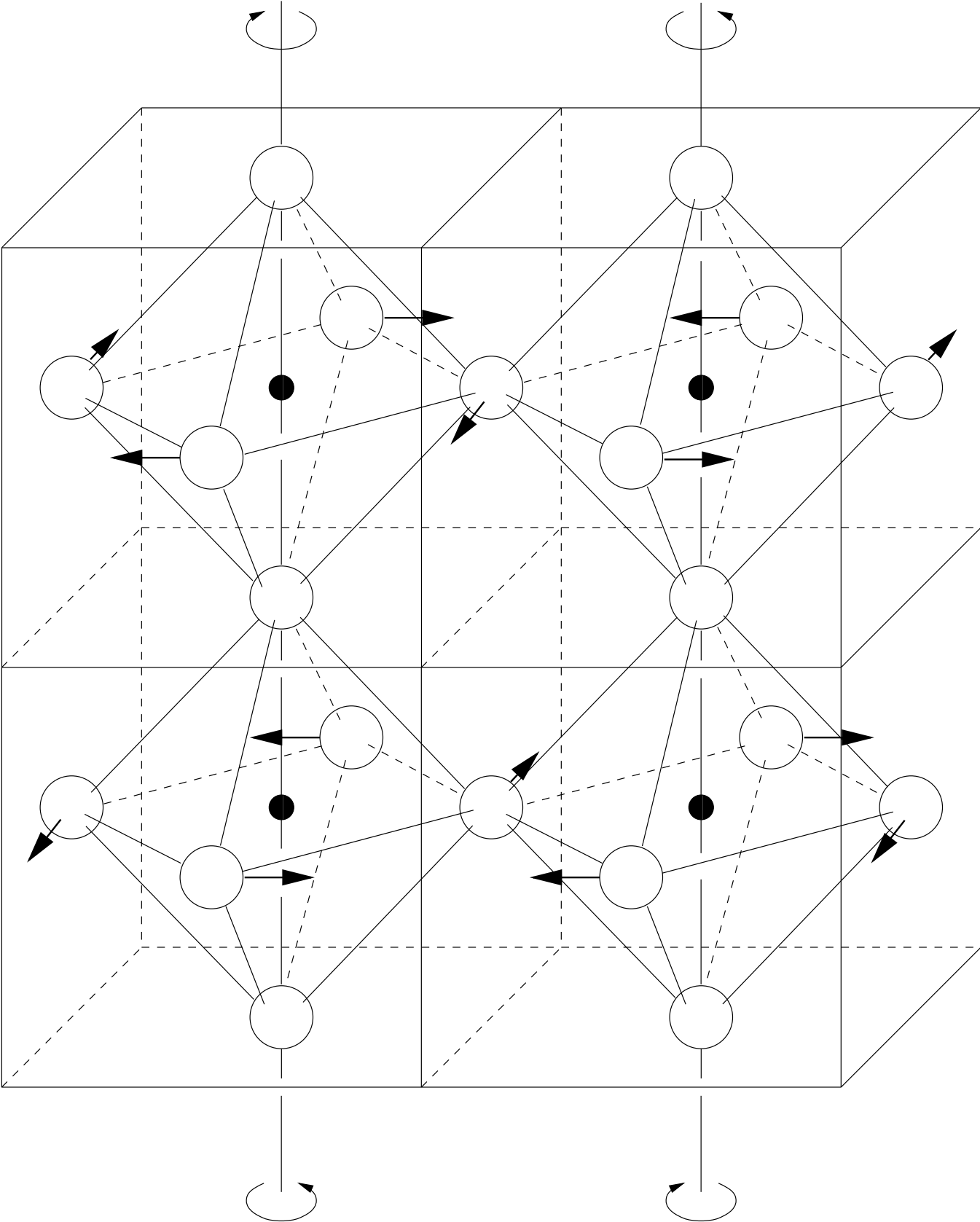
Present	PW <sup>a</sup>	Exp. <sup>b</sup> (300 K)
TO modes:		
100i	41i	Soft
151	165	175
219		IR-silent
522	546	545
LO modes:		
146 <sup>A</sup> 146 <sup>B</sup>	158	171
439 <sup>A</sup> 449 <sup>B</sup>	454	474
751 <sup>A</sup> 832 <sup>B</sup>	829	795

<sup>a</sup>Reference [16].

<sup>b</sup>Reference [25].

<sup>A</sup>Using Eq.(7) and the calculated value  $\varepsilon_\infty=6.63$ .

<sup>B</sup>Using Eq.(7) and  $\varepsilon_\infty=5.18$  extracted from experiment.





This figure "fig3.jpg" is available in "jpg" format from:

<http://arxiv.org/ps/cond-mat/9703240v1>